Fate mapping melanoma persister cells through regression and into recurrent disease in adult zebrafish

Jana Travnickova[1,2], Sarah Muise[1,2], Sonia Wojciechowska[1,2,3], Alessandro Brombin[1,2], Zhiqiang Zeng[1,2], Cameron Wyatt[1], E. Elizabeth Patton[1,2,4]

1. MRC Human Genetics Unit, Institute of Genetics and Cancer, University of Edinburgh, Western General Hospital Campus, EH4 2XU, Edinburgh, United Kingdom.

2. CRUK Edinburgh Centre, Institute of Genetics and Cancer, University of Edinburgh, Western General Hospital Campus, EH4 2XU, Edinburgh, United Kingdom.

3. Current address: Department of Paediatric Oncology, Dana-Farber Cancer Institute, Harvard Medical School, Boston, MA, 02215, USA

4. Corresponding author: e.patton@ed.ac.uk
   ORCID ID: 0000-0002-2570-0834

Abstract

Melanoma heterogeneity and plasticity underlie therapy resistance. Some tumour cells possess innate resistance while others reprogramme during drug exposure and survive to form persister cells, a source of potential cancer cells for recurrent disease. Tracing individual melanoma cell populations through tumour regression and recurrent disease remains largely unexplored, in part, because complex animal models are required for live imaging of cell populations over time. Here, we apply tamoxifen-inducible *cre*^{ERt2}*/loxP* lineage tracing to a zebrafish model of MITF-dependent melanoma regression and recurrence to image and trace cell populations *in vivo* through disease stages. Using this strategy, we showed that melanoma persister cells at the minimal residual disease site originate from the primary tumour. Next, we fate mapped rare MITF-independent persister cells and demonstrate that these cells directly contribute to progressive disease. Multiplex immunohistochemistry confirmed MITF-independent persister cells give rise to Mitfa+ cells in recurrent disease. Taken together, our work reveals a direct contribution of melanoma persister cell populations to recurrent disease, and provides a resource for lineage tracing methodology in adult zebrafish cancer models.

Key words:

Zebrafish, lineage tracing, fate mapping, melanoma, persister cells, recurrent disease

Summary statement:

We fate map melanoma cells from the primary tumour into a persister cell state and show that persister cells directly contribute to recurrent disease.

INTRODUCTION

Melanoma, a deadly cancer of pigment producing melanocytes, ranks amongst the highest for genetic and transcriptional heterogeneity (Rambow et al., 2019; Travnickova and Patton, 2021) . Therapy resistance remains a major challenge for patients with melanoma, with partial or short-term responses characteristic of targeted therapy, eventually resulting in tumour relapse (Patton et al., 2021; Shen et al., 2020b). This resistance can be intrinsic, in which pre-existing primary tumour cell states directly confer resistance, or acquired, whereby melanoma cells develop resistance upon drug exposure either by acquiring new genetic mutations or adapting their transcriptional state (Marin-Bejar et al., 2021; Marine et al., 2020; Shen *et al.*, 2020b). These resistance mechanisms likely occur concurrently, and contribute to the high heterogeneity within melanoma and the persister cell states at the minimal residual disease (MRD) site.

Recently, using single cell RNA sequencing (scRNA-seq), we and others have demonstrated high transcriptional heterogeneity and distinct cell states in the primary tumour and MRD, including states with low-to-no expression of pigmentation lineage markers such as melanocyte inducing transcription factor (MITF)-independent populations (Baron et al., 2020; Ennen et al., 2015; Gerber et al., 2017; Rambow et al., 2018; Tirosh et al., 2016; Travnickova et al., 2019). These studies have identified multiple melanoma cell states that have been proposed to drive tumour recurrence, while others are of unknown contribution to disease progression (Travnickova and Patton, 2021). While revealing new concepts about melanoma transcriptional cell states, these studies reflect only a single or few time points, and are thereby limited in what can be understood about the behaviour of individual cell populations over time.

This limitation is particularly critical in the context of cell plasticity in cancer models. Advances in imaging technologies coupled with lineage tracing methods in zebrafish models now enable the fate mapping of cell populations over time (Mosimann et al., 2011; Pan et al., 2013). The power of an inducible lineage tracing system is illustrated by advances in understanding of organ development and tissue homeostasis in zebrafish (Carney and Mosimann, 2018;

28 Thunemann et al., 2017). For example, lineage tracing experiments using the general neural
29 crest marker *sox10* or the recently established melanocyte stem cell marker *tfap2b* provided
30 proof of the existence of multipotent melanocyte precursors during early embryonic
31 development and their contribution to adult zebrafish pigment cell patterning (Brombin et al.,
32 2022; Singh et al., 2016). Similarly, a conditional *cre/loxP* recombination system demonstrated
33 the hierarchy of neuroepithelial progenitors and the functional heterogeneity of neural stem
34 cells in the vertebrate adult brain using neural lineage specific markers (Galant et al., 2016;
35 Than-Trong et al., 2020). Furthermore, multispectral lineage tracing revealed the mechanism
36 behind myotome generation (Nguyen et al., 2017). The regenerative capacities of zebrafish
37 combined with an inducible lineage tracing system have been instrumental in understanding
38 the cell origin and lineage restrictions in regenerated organs such as lesioned heart, fins or
39 spinal cord (Briona et al., 2015; Jopling et al., 2010; Tornini et al., 2017). Recently, multicolour
40 tracing has been combined with mosaic mutagenesis using CRISPR-Cas9 in a novel
41 technique called TWISTR (tissue editing with inducible stem cell tagging via recombination) to
42 show that the fitness of mutant clones is controlled by resistance to inflammation (Avagyan et
43 al., 2021). Despite these advances, the application of tamoxifen to control the temporal and
44 spatial activation of Cre (Cre^{ERt2}) in adult zebrafish cancer models has been hampered by
45 technical challenges, such as lack of established protocols and tamoxifen toxicity.

46 Here, we adapt and optimise the inducible *ubi:Switch* lineage tracing system (Mosimann *et*
47 *al.*, 2011) for use in an adult zebrafish cancer model to fate map cells through melanoma
48 growth, regression and recurrence. For the first time, we directly capture melanoma cell
49 switching from MITF-independent persister cells to Mitfa positive cells to contribute to
50 recurrent disease *in vivo*. Our work supports the concept that targeting persister cells will be
51 critical to delay or prevent recurrent disease.

52

53

54 **RESULTS**

55 **Conditional tamoxifen induced fluorophore switch in adult zebrafish melanoma**

56 We have previously developed a conditional MITF-dependent zebrafish melanoma model
57 (*Tg(mitfa:BRAF^{V600E});mitfa^{vc7};tp53^{M214K}*), in which melanoma regresses and recurs
58 concurrently with the changes in MITF activity controlled by temperature (Travnickova et al.,
59 2019). In this model, MITF activity is controlled by a temperature sensitive splicing mutation
60 in the *mitfa* gene (*mitfa^{vc7}*). At the lower permissive temperature, MITF activity is on and
61 promotes tumourigenesis, while at the higher temperature *mitfa* RNA is still expressed but is
62 not spliced correctly and thereby MITF activity is abolished. Turning off MITF activity results
63 in tumour regression with remaining persister cells at the MRD site (Travnickova *et al.*, 2019).

64 To trace melanoma cells through disease states, we first set out to establish an inducible
65 *cre/loxP* system on the MITF-dependent melanoma background. To this end, we expressed
66 *cre^{ERt2}* from the *mitfa* promoter to generate a transgenic *Tg(mitfa:cre^{ERt2})* line and crossed this
67 with a *ubi:Switch* reporter line (Mosimann *et al.*, 2011). This experimental design would enable
68 us to induce a green-to-red (GFP-to-mCherry) permanent fluorophore switch in *mitfa:cre^{ERt2}*
69 expressing melanoma cell populations at a defined time point in melanoma disease
70 progression (**Fig. 1A, B**).

71 We found that 4 µM tamoxifen treatment of adult zebrafish by immersion for three consecutive
72 nights (11-hour-treatment, 13-hour-recovery) was successful for *cre^{ERt2}/loxP* recombination
73 without toxicity (**Fig 1B**, **Fig. 2A**). We chose tamoxifen over 4-hydroxytamoxifen (4-OHT) for
74 its increased solubility in dimethylsulfoxide (DMSO) which is well tolerated by adult zebrafish.
75 The treatment was completed overnight to align with the natural light-dark cycle of the fish and
76 to prevent phototoxicity of tamoxifen (Wang et al., 2009). By three days post tamoxifen
77 treatment course, we could detect mCherry in the primary tumour, but not in DMSO treated
78 controls (**Fig.2B**, **Fig. S1A**). Using confocal microscopy, we validated the presence of
79 individual clusters of mCherry+ melanoma cells in tamoxifen treated tumours only (**Fig. 2C-**

80 **D**). Immunostaining of melanoma sections with a mCherry antibody showed that mCherry+
81 cells were present both at the surface of the tumour and in the invading melanoma cells along
82 muscle fibres thus confirming the efficiency of this protocol to fate map cells throughout the
83 body of the melanoma tumour (**Fig. 2E, F**).

84 Having established the system in a single colour switch reporter line, we wanted to test if our
85 method was applicable to the multicolour system of fate mapping. To this end, we crossed the
86 *Tg(mitfa:cre^{ERt2})* fish with the *ubi:zebrabow* transgenic line (Pan et al., 2013) to evaluate colour
87 changes in *cre^{ERt2}* expressing cells to a stochastic combinatorial expression of three
88 fluorophores upon tamoxifen treatment: CFP (Cerulean), YFP and RFP (dTomato) (**Fig. 2G**).
89 Indeed, 19 days after tamoxifen treatment, we could detect all three fluorophores within an
90 early stage melanoma and following tumour progression further, we detected expansive
91 growth for a YFP+ cell population, forming the basis of a nodular melanoma after tamoxifen
92 treatment only (**Fig. 2H, Fig. S1B**). While we did not evaluate clonal evolution in melanoma
93 progression (as it would require more rigorous analysis of colour switch stochasticity), this
94 experiment demonstrated the potential for our tamoxifen treatment protocol for application in
95 clonal analysis studies in zebrafish cancer models.

96

97 **Melanoma persister cells originate from the primary tumour**

98 Next, we used our conditional MITF-dependent BRAF^{V600E} p53^{M214K} model to trace melanoma
99 cells from the primary tumour as it regresses and thereby determine if the cells detected at
100 the MRD site originate from the primary tumour (**Fig. 3A**). Tamoxifen treatment of early-stage
101 melanoma resulted in a GFP-to-mCherry switch in tumour lesions that was absent in DMSO
102 treated animals (**Fig. 3B-C**). Following a period of tumour growth, we transferred fish to a
103 higher temperature and to turn off MITF activity and cause tumour regression. Strikingly, at
104 the MRD site, we could detect mCherry+ persister cells in tamoxifen treated fish (**Fig. 3B-C**).
105 Confocal microscopy and quantification confirmed that tamoxifen treated fish showed

106 significantly greater mCherry signal at the MRD site compared to DMSO treated fish (**Fig. 3D-**
107 **E**). Whilst most DMSO treated fish did not show any mCherry signal, we could detect it in a
108 small proportion of the control fish (**Fig. 3E**). This may be due to *cre* expression (leakage) in
109 those tissues where *mitfa* expression is very high (for example in some nodular tumours as
110 we have described previously (Travnickova et al., 2019)). Immunostaining of regressed
111 melanoma tissue sections validated the presence of mCherry+ persister cells at the MRD site
112 (**Fig. 3F**). These data indicate that primary melanoma cells directly give rise to persister cells
113 at the MRD site.

114

115 **Melanoma persister cells directly contribute to tumour recurrence**

116 Next, we asked if the tamoxifen induced GFP-to-mCherry switch could also be applied to
117 melanoma persister cells in the MRD site. We transferred our melanoma fish to a higher water
118 temperature to prevent the correct splicing of *mitfa* (and to thereby turn off Mitfa protein
119 activity) to cause melanoma regression. Because the *mitfa*^{vc7} mutation is an RNA splicing
120 mutation, the expression of *mitfa* or reporters under the control of *mitfa* (e.g. *mitfa:GFP*;
121 *mitfa:cre*^{ERt2}) are not affected at the restrictive temperature. Once the melanoma had fully
122 regressed, we treated the fish with tamoxifen (**Fig. 4A**). We detected mCherry+ cells 6 days
123 after the start of tamoxifen treatment at the regression site (**Fig. 4B-C**). Using confocal
124 microscopy, we were able to validate the presence of mCherry+ cells in the tamoxifen treated
125 group (**Fig. 4D**), that were morphologically similar to our previous observations using
126 *Tg(mitfa:GFP)* transgenic line (Travnickova et al., 2019).

127 Melanoma persister cells have been proposed to contribute to disease recurrence and drug
128 resistance (Marin-Bejar *et al.*, 2021; Rambow *et al.*, 2018; Shen et al., 2020a; Travnickova *et*
129 *al.*, 2019; Vendramin et al., 2021), but this has not been demonstrated in an animal model
130 using lineage tracing. Having validated the successful GFP-to-mCherry switch at the MRD
131 site, we next sought to follow the persister cells during recurrence. Once again, we performed

132 tamoxifen treatment and detected GFP-to-mCherry switched persister cells at the MRD site.
133 We then restored MITF activity by lowering the water temperature and followed melanoma
134 recurrence. Over 50 days, the mCherry+ cells continuously increased concomitantly with
135 melanoma recurrence (**Fig. 5A-B**). This demonstrates that persister cells directly contribute to
136 recurrent disease.

137 Confocal microscopy enabled us to visualise the tumours at cellular resolution, showing fields
138 of mCherry+ melanoma cells in recurrent disease (**Fig. 5C**). Quantification of the mCherry+
139 fluorescence indicated that most recurrent disease sites expressed mCherry (**Fig.5D**). For one
140 sample, we found the fluorescence was hindered by strong pigmentation. Given this, we
141 validated the presence of mCherry+ cells in this and other recurrent tumours using flow
142 cytometry and could clearly detect mCherry even in highly pigmented samples (**Fig. 5E**).

143

144 **Transcriptional plasticity of melanoma persister cells in recurrent disease**

145 We hypothesised that persister cells directly lead to recurrent disease by transitioning from an
146 MITF-independent to a Mitfa+ state. We have previously shown that persister cells do not
147 express Mitfa protein, but maintain a neural crest identity and express Sox10 (Travnickova et
148 al., 2019). We applied multiplex immunohistochemistry (MIHC) on sections of the recurred
149 tumours to determine the protein expression levels of Mitf and other melanoma markers within
150 recurrent disease (**Fig. 6A-D**). MIHC allows sequential staining and stripping of several
151 antibodies on the same slide (Pirici et al., 2009). We used an antibody against the mCherry
152 protein to label the "switched" cells in tamoxifen treated fish compared to DMSO control,
153 together with antibodies against the melanoma markers Sox10 and Mitfa (**Fig. 6B-D**). As
154 anticipated, recurred tumours from DMSO controls lacked mCherry signal in Sox10+ and Mitf+
155 tumour cells (**Fig. 6B, B'**). By overlaying the images of mCherry staining with Sox10 and Mitf
156 staining we could demonstrate that the mCherry+ cells within the tamoxifen treated recurred
157 tumour expressed both Sox10 and Mitf (**Fig. 6D'**). These results indicate that melanoma

158 persister cells undergo a cell state switch from MITF-independent to Mitfa+ expressing cells,
159 regaining features of the primary tumour, and providing direct evidence of tumour cell
160 transcriptional plasticity *in vivo*.

161

162 **DISCUSSION**

163 Transcriptional heterogeneity underlies the high levels of tumour cell plasticity in melanoma.
164 Here, we apply fate mapping and MIHC to tumour cell populations through melanoma disease
165 states to show that (1) persister cells originate from the primary tumour; (2) persister cells
166 directly contribute to melanoma recurrence; and (3) persister cells exhibit plasticity from a
167 MITF-independent state to Mitfa expressing melanoma cells in recurrent disease. Thus,
168 persister cells will be a critical drug target for delaying (or even preventing) melanoma
169 recurrent disease.

170 Our system offers the opportunity to understand how individual cell states, and indeed even
171 individual cells, contribute to drug resistance and tumour progression in zebrafish cancer
172 models. Lessons from mouse models indicate that the efficiency of recombination is largely
173 dependent on the expression level and pattern of the chosen promoter and thus the tamoxifen
174 protocol often needs to be adapted for each *cre*^{ERt2} line (Ellisor and Zervas, 2010; Jahn et al.,
175 2018). In particular, the Bally-Cuif group recently established a 4-OHT protocol for mosaic
176 recombination using short-term drug exposure and long-term multiple-day immersion for
177 maximal recombination, similar to our approach (Than-Trong et al., 2020). Hence, as inducible
178 lineage tracing methods become more widely applied in zebrafish adults, the zebrafish
179 community will benefit from ensuring tamoxifen protocols for each promoter are accessible to
180 the community.

181 Here, we showed the fate mapping of *mitfa:cre*^{ERt2} expressing melanoma population, which
182 represents a major portion of melanoma cells in our model. MITF is one of the universal
183 diagnostic markers of cutaneous melanoma based on its expression in most melanoma cells

184 (Compton et al., 2015). Previously, we and others have demonstrated the level and
185 importance of transcriptional heterogeneity not only in the primary tumour but also in the
186 persister cells at the MRD site (Marin-Bejar *et al.*, 2021; Rambow *et al.*, 2018; Shen *et al.*,
187 2020b; Travnickova *et al.*, 2019; Wouters et al., 2020). This system has the potential to allow
188 fate mapping of these different transcriptional cell states at the MRD site and evaluate their
189 contribution to disease progression and response to drug treatment. This can be achieved
190 using cell state specific markers to recombine a subpopulation of the tumour at the desired
191 stage.

192 In conclusion, we have successfully applied and validated an inducible *cre*^{ERt2}*/loxP* lineage
193 tracing system in an adult zebrafish melanoma model to follow cell states through disease
194 stages. Combining fate mapping with live imaging and MIHC, we provide direct evidence for
195 the contribution of cells at the MRD site to tumour recurrence, whilst simultaneously
196 demonstrating their MITF-independent to Mitfa+ cell state shift. This system has the potential
197 for widespread usage in the study of cancer cell plasticity over time and in the evolution of
198 therapy resistance.

199

200 **METHODS**

201 **Experimental Models and Husbandry**

202 Zebrafish were maintained in accordance with UK Home Office regulations, UK Animals
203 (Scientific Procedures) Act 1986, amended in 2013, and European Directive 2010/63/EU
204 under project license 70/8000 and P8F7F7E52. All experiments were approved by the Home
205 office and AWERB (University of Edinburgh Ethics Committee).

206 Fish stocks used were: *mitfa*^{vc7} (Johnson et al., 2011; Zeng et al., 2015), *Tg(mitfa-BRAF*^{V600E}*),*
207 *tp53*^{M214K}*(lf)* (Patton et al., 2005)*, Tg(ubb:loxP-EGFP-loxP-mCherry)* (referred as *ubi:Switch*)
208 (Mosimann *et al.*, 2011), *Tg(ubb:lox2272-loxP-Tomato-lox2272-Cerulean-loxP-YFP)* (referred

209 as *ubi:zebrabow*; (Pan *et al.*, 2013), *Tg(mitfa:cre^{ERt2})* (this study). Combined transgenic and
210 mutant lines were generated by crossing. Adult fish were maintained either at 28.5°C, 25°C or
211 32°C under 14:10 light:dark cycles.

212 **Generation of zebrafish transgenic line *mitfa:cre^{ERt2}***

213 Cre^{ERt2} was amplified by gateway PCR using pCGA_Cre^{ERt2} (Addgene plasmid #14797) as
214 template. A nuclear localization signal (NLS) was added to its N terminal. The gateway primer
215 sequences are CreERt2gateF 5'-
216 GGGGACAAGTTTGTACAAAAAAGCAGGCTGCCACCATGCCCAAGAAGAAGAGGAAGGT
217 GTCCAATTTACTGACCGTACACC-3' and CreERt2gateR: 5'
218 GGGGACCACTTTGTACAAGAAAGCTGGGTTCAAGCTGTGGCAGGGAAAC -3'. The PCR
219 product was cloned into pDONOR221 resulting in pME-Cre^{ERt2}, a middle entry vector. cre^{ERt2}
220 was then cloned together with the 2.1kb zebrafish *mitfa* promoter into *pDestTol2CG2*
221 destination vector by the Tol2kit gateway cloning method (Kwan et al., 2007), resulting in the
222 *pEXPmitfa-Cre^{ERt2}* expression vector. For selection purposes, the construct contains an
223 additional GFP coding sequence expressed from the heart specific *cmlc2* promoter. Two nl of
224 mixed *pEXPmitfa-Cre^{ERt2}* plasmid and *Tol2* mRNA (25ng/µl and 35ng/µl respectively) were
225 injected into 1-cell stage zebrafish embryos. Zebrafish embryos with the GFP transgenic
226 marker in the heart were selected and grown to adulthood, then bred with wildtype fish to
227 establish stable lines

228 **Genotyping**

229 Zebrafish were genotyped using DNA extracted from fin clipped tissue using DirectPCR lysis
230 reagent (Viagen) complemented with 0.1 mg.ml^{-1} proteinase K. Polymerase chain reaction
231 (PCR) was used to establish the mutant allele status *p53^{M214K}* and to verify the presence of
232 transgene mitfa-*BRAF^{V600E}* as described in detail before (Wojciechowska et al., 2016).

233

234 **Water temperature shifts**

235 To induce melanoma regression, selected adult melanoma-prone fish homozygous for *mitfa*^{vc7}
236 mutation were transferred to tanks with heaters that kept the water temperature at 32°C
237 compared to standard system temperature of 28°C. To allow melanoma recurrence, regressed
238 fish were transferred to tanks at room temperature (24 - 26°C), while monitored daily for tumor
239 progression and health condition of the fish. Fish were always imaged prior to transfer from
240 one temperature to another, then imaged regularly to track their progression and monitored
241 daily.

242 **Tamoxifen treatment**

243 Tamoxifen treatment protocol was adapted from works of Gemberling *et al* and Pinzon-Olejua
244 *et al*. (Gemberling et al., 2015; Pinzon-Olejua et al., 2017). Tamoxifen stock solution (Cayman
245 Chemicals or Fisher Scientific) was prepared by dissolving powder in DMSO to reach 10mM
246 concentration. We prepared fresh stock for each round of treatment on day 0 for the whole 3-
247 day-treatment course and stored at -20°C in 200-250 µl aliquots. Tamoxifen stock solution (or
248 corresponding DMSO volume as a control) was diluted with 500 ml E3 medium (5mM NaCl,
249 0.17mM KCl, 0.33mM $CaCl_2$, 0.33mM $MgSO_4$) in a fish carrier tank and fish immersed in the
250 solution for 11-12 hours overnight (protected from light using black chamber box or aluminium)
251 with drug pause during the day for 3 consecutive nights. For the tamoxifen treatment of
252 regressed melanoma fish, the carrier tanks with fish immersed in the tamoxifen or DMSO were
253 kept in a water bath set at 31°C to ensure the continuous suppression of MITF activity.

254 **Live imaging of adult zebrafish**

255 Fish were briefly anaesthetized in tricaine solution (MS-222, 0.1 $g.l^{-1}$), placed onto a Petri dish
256 while immersed in the tricaine solution and imaged using a Nikon COOLPIX5400 camera
257 attached to a brightfield microscope (Nikon SMZ1500). Each fish was imaged using 3
258 consecutive photo shots that were later merged together using Adobe Photoshop automerge
259 function. For fluorescent imaging, anaesthetized fish were imaged under the Leica M165FC

260 or Leica MZFIII stereomicroscopes equipped with Retiga R1 camera operated via µManager
261 software (Edelstein et al., 2010). Images were taken using UV, GFP and mCherry fluorescent
262 filters. The fluorescent images were processed using Fiji software version 2.1.0 (Schindelin et
263 al., 2012) for pseudocolouring and adjusting minimal and maximal intensity.

264 **Zebrafish tissue confocal imaging**

265 For confocal microscopy, fish were culled by overdose of anesthetic (MS-222 1 $g.l^{-1}$, followed
266 by death confirmation) and embedded in 1% low-melting temperature point agarose
267 (Invitrogen) with the tumour or regressed tissue oriented to the bottom of six well glass bottom
268 plate (Cellvis). Images were obtained under Andor Dragonfly spinning disk confocal
269 microscope equipped with Andor Zyla sCMOS camera through 20x air immersion objective
270 with 2048x2048 px resolution and 1 µm interval.

271 **Image processing and Fluorescence quantification**

272 Confocal acquisitions were processed using Fiji software version 2.1.0 (Schindelin *et al.*,
273 2012). Standard-deviation intensity projections of all z-slices were used except for
274 fluorescence intensity quantification where average intensity projections were used.
275 Fluorescence intensity has been measured as described by McCloy et al (McCloy et al., 2014).
276 Briefly, average intensity projections of z-stack acquired using Andor Dragonfly spinning disk
277 confocal microscope were split by channel to select mCherry only. Intensity was then
278 measured of the whole imaged region and small region without any tissue used to determine
279 background. To calculate fluorescence intensity, corrected total cell fluorescence (CTCF) was
280 calculated by subtracting the background fluorescence intensity. Any negative value was
281 replaced by 0. Graphs summarizing the fluorescence intensity quantification were made using
282 R software version 4.0.3 via R studio interface version 1.1.456 equipped with ggplot2 package
283 (R-Core-Team, 2020; RStudio-Team, 2016; Wickham, 2016).

284

285 **Fluorescence activated cell sorting**

286 Adult tamoxifen treated or DMSO control fish with recurred tumours were culled using
287 overdose of tricaine (MS-222, 1 $g.l^{-1}$ followed by death confirmation). Tumours were
288 individually dissected and chopped using sterile No.9 blade scalpels. Samples were then
289 dissociated with 0.25 $mg.ml^{-1}$ liberase TL (Roche) for 15 minutes at room temperature while
290 inverting the tube, re-suspended in FACSmax cell dissociation solution (Genlatis) and filtered
291 through 40µm cell strainer. Samples were sorted by a FACSAria2 SORP instrument (BD
292 Biosciences UK) equipped with 405nm, 488nm and 561 nm lasers. Green fluorescence was
293 detected using GFP filters 525/50 BP and 488 nm laser, red fluorescence using mCherry filters
294 610/20 BP and 561 nm laser and live cells selected as DAPI negative using DAPI filters 450/20
295 BP and 405 nm laser. Data were analyzed using FlowJo software (BD Biosciences) version
296 10.8.1.

297 **Histology**

298 Fish samples were collected, fixed and processed as described in detail in (Wojciechowska *et*
299 *al.*, 2016). Briefly, tissue was fixed by immersion in 4% PFA at 4°C with agitation for 3 days,
300 decalcified in 0.5M EDTA (pH 8) at 4°C with agitation for 5 days and then stored in 70% ethanol
301 at 4°C. To obtain sections for pathology analysis, tissue was processed in 95% ethanol,
302 absolute alcohol, xylene and paraffin, embedded in blocks, cut into 5 µm thick sections and
303 placed onto glass slides. Haematoxylin and eosin staining and immunohistochemistry were
304 performed as described in detail in (Wojciechowska *et al.*, 2016). The slides were imaged
305 using Hamamatsu Nanozoomer SlideScanner and the images were processed using NDP.3
306 software.

307 **Immunofluorescence staining**

308 FFPE sections were deparaffinised in xylene and gradually rehydrated through baths of
309 ethanol of decreasing concentrations. Sections were bleached in 1% KOH/3% H_2O_2 solution
310 for 15 minutes prior to subjected to heat mediated antigen retrieval in citrate buffer (0.01M,

311 pH6). Sections were blocked in 10% goat serum for 1 hour and incubated with primary
312 antibody mCherry (Abcam, ab125096) at dilution 1:3,000 overnight at 4 °C. After PBST
313 washes, sections were incubated with 546 AlexaFluor Goat anti-mouse secondary antibody
314 at 1:500 dilution (Invitrogen) and DAPI (Sigma, 1:500 dilution) for 30 min in dark at room
315 temperature and mounted in hydrophilic mounting medium prior imaging. Sections were
316 imaged using Andor Dragonfly confocal microscope equipped with Andor Zyla sCMOS
317 camera using 20x air immersion objective.

318 **Multiplex Immunohistochemistry**

319 FFPE sections were deparaffinised with xylene before gradual rehydration and bleached in a
320 1% KOH/3% H_2O_2 solution for 15 minutes. Slides were then stained with haematoxylin,
321 mounted in hydrophilic mounting media and imaged using a Hamamatsu NanoZoomer slide
322 scanner. After coverslip removal, slides were subjected to heat-mediated antigen retrieval in
323 citrate buffer (0.01M, pH6) for 7 minutes. The sections were then incubated in serum-free
324 protein blocking solution (DAKO) for 30 minutes at room temperature and incubated in primary
325 antibody overnight at 4°C. Following TBST washes, the sections were incubated in HRP
326 rabbit/mouse secondary antibody (DAKO Real EnVision kit) for 30 minutes at room
327 temperature. Antibody staining was revealed via incubation in AEC chromogen (Abcam) for
328 5-30 minutes. Following each antibody revealing, the slides were again mounted in hydrophilic
329 mounting media and imaged using a Hamamatsu NanoZoomer slide scanner. The slides
330 were then de-coverslipped and underwent chromogenic de-staining in an alcohol gradient and
331 subsequent antibody stripping via a 75 minute incubation in a solution glycine-SDS, pH 2 at
332 50 ºC, before the next blocking and antibody round (adapted from (Pirici *et al.*, 2009; Tsujikawa
333 et al., 2017)). The following antibodies were used for multiplex IHC: Sox10 (Abcam, ab229331,
334 1:4,000), mCherry (Abcam, ab125096, 1:4,000) and Mitf (Sigma, SAB2702433, 1:1,000)

335

336 **Statistical analysis**

Sample distribution was evaluated using Shapiro-Wilk test. As the samples exhibited non-gaussian distribution, statistical evaluation was performed using nonparametric Wilcoxon test. We set up the threshold to P=0.05 to be considered as statistically significant with the following symbols: ** $p<0.01$; * $p<0.05$. Statistical analysis was performed using R software version 4.0.3 through R studio interface version 1.1.456 (R-Core-Team, 2020; RStudio-Team, 2016).

Declaration of Interests

E.E.P. is the Editor-in-Chief *at Disease Models & Mechanisms* but is not included in any aspect of the editorial handling of this article.

Acknowledgements

We are grateful to the MRC HGU Zebrafish Facility for zebrafish management and husbandry, Elisabeth Freyer and the MRC HGU FACS facility, Ann Wheeler and the IGC Imaging Facility for supporting the imaging experiments, and Adelaide Young for help with flow cytometry interpretation. EEP is funded by MRC HGU Programme (MC_UU_00007/9), the European Research Council (ZF-MEL-CHEMBIO-648489), and Melanoma Research Alliance (687306).

REFERENCES

Avagyan, S., Henninger, J.E., Mannherz, W.P., Mistry, M., Yoon, J., Yang, S., Weber, M.C., Moore, J.L., and Zon, L.I. (2021). Resistance to inflammation underlies enhanced fitness in clonal hematopoiesis. Science *374*, 768-772. 10.1126/science.aba9304.

Baron, M., Tagore, M., Hunter, M.V., Kim, I.S., Moncada, R., Yan, Y., Campbell, N.R., White, R.M., and Yanai, I. (2020). The Stress-Like Cancer Cell State Is a Consistent Component of Tumorigenesis. Cell Syst *11*, 536-546 e537. 10.1016/j.cels.2020.08.018.

Briona, L.K., Poulain, F.E., Mosimann, C., and Dorsky, R.I. (2015). Wnt/ss-catenin signaling is required for radial glial neurogenesis following spinal cord injury. Dev Biol *403*, 15-21. 10.1016/j.ydbio.2015.03.025.

Brombin, A., Simpson, D.J., Travnickova, J., Brunsdon, H., Zeng, Z., Lu, Y., Young, A.I.J., Chandra, T., and Patton, E.E. (2022). Tfap2b specifies an embryonic melanocyte stem cell that retains adult multifate potential. Cell Rep *38*, 110234. 10.1016/j.celrep.2021.110234.

Carney, T.J., and Mosimann, C. (2018). Switch and Trace: Recombinase Genetics in Zebrafish. Trends Genet *34*, 362-378. 10.1016/j.tig.2018.01.004.

Compton, L.A., Murphy, G.F., and Lian, C.G. (2015). Diagnostic Immunohistochemistry in Cutaneous Neoplasia: An Update. Dermatopathology (Basel) *2*, 15-42. 10.1159/000377698.

Edelstein, A., Amodaj, N., Hoover, K., Vale, R., and Stuurman, N. (2010). Computer control of microscopes using microManager. Curr Protoc Mol Biol *Chapter 14*, Unit14 20. 10.1002/0471142727.mb1420s92.

Ellisor, D., and Zervas, M. (2010). Tamoxifen dose response and conditional cell marking: is there control? Mol Cell Neurosci *45*, 132-138. 10.1016/j.mcn.2010.06.004.

Ennen, M., Keime, C., Kobi, D., Mengus, G., Lipsker, D., Thibault-Carpentier, C., and Davidson, I. (2015). Single-cell gene expression signatures reveal melanoma cell heterogeneity. Oncogene *34*, 3251-3263. 10.1038/onc.2014.262.

Galant, S., Furlan, G., Coolen, M., Dirian, L., Foucher, I., and Bally-Cuif, L. (2016). Embryonic origin and lineage hierarchies of the neural progenitor subtypes building the zebrafish adult midbrain. Dev Biol *420*, 120-135. 10.1016/j.ydbio.2016.09.022.

Gemberling, M., Karra, R., Dickson, A.L., and Poss, K.D. (2015). Nrg1 is an injury-induced cardiomyocyte mitogen for the endogenous heart regeneration program in zebrafish. Elife *4*. 10.7554/eLife.05871.

Gerber, T., Willscher, E., Loeffler-Wirth, H., Hopp, L., Schadendorf, D., Schartl, M., Anderegg, U., Camp, G., Treutlein, B., Binder, H., and Kunz, M. (2017). Mapping heterogeneity in patient-derived melanoma cultures by single-cell RNA-seq. Oncotarget *8*, 846-862. 10.18632/oncotarget.13666.

Jahn, H.M., Kasakow, C.V., Helfer, A., Michely, J., Verkhratsky, A., Maurer, H.H., Scheller, A., and Kirchhoff, F. (2018). Refined protocols of tamoxifen injection for inducible DNA recombination in mouse astroglia. Sci Rep *8*, 5913. 10.1038/s41598-018-24085-9.

Johnson, S.L., Nguyen, A.N., and Lister, J.A. (2011). mitfa is required at multiple stages of melanocyte differentiation but not to establish the melanocyte stem cell. Dev Biol *350*, 405-413. 10.1016/j.ydbio.2010.12.004.

Jopling, C., Sleep, E., Raya, M., Marti, M., Raya, A., and Izpisua Belmonte, J.C. (2010). Zebrafish heart regeneration occurs by cardiomyocyte dedifferentiation and proliferation. Nature *464*, 606-609. 10.1038/nature08899.

Kwan, K.M., Fujimoto, E., Grabher, C., Mangum, B.D., Hardy, M.E., Campbell, D.S., Parant, J.M., Yost, H.J., Kanki, J.P., and Chien, C.B. (2007). The Tol2kit: a multisite gateway-based construction kit for Tol2 transposon transgenesis constructs. Dev Dyn *236*, 3088-3099. 10.1002/dvdy.21343.

Marin-Bejar, O., Rogiers, A., Dewaele, M., Femel, J., Karras, P., Pozniak, J., Bervoets, G., Van Raemdonck, N., Pedri, D., Swings, T., et al. (2021). Evolutionary predictability of genetic versus nongenetic resistance to anticancer drugs in melanoma. Cancer Cell *39*, 1135-1149 e1138. 10.1016/j.ccell.2021.05.015.

Marine, J.C., Dawson, S.J., and Dawson, M.A. (2020). Non-genetic mechanisms of therapeutic resistance in cancer. Nat Rev Cancer *20*, 743-756. 10.1038/s41568-020-00302-4.

McCloy, R.A., Rogers, S., Caldon, C.E., Lorca, T., Castro, A., and Burgess, A. (2014). Partial inhibition of Cdk1 in G 2 phase overrides the SAC and decouples mitotic events. Cell Cycle *13*, 1400-1412. 10.4161/cc.28401.

Mosimann, C., Kaufman, C.K., Li, P., Pugach, E.K., Tamplin, O.J., and Zon, L.I. (2011). Ubiquitous transgene expression and Cre-based recombination driven by the ubiquitin promoter in zebrafish. Development *138*, 169-177. 10.1242/dev.059345.

Nguyen, P.D., Gurevich, D.B., Sonntag, C., Hersey, L., Alaei, S., Nim, H.T., Siegel, A., Hall, T.E., Rossello, F.J., Boyd, S.E., et al. (2017). Muscle Stem Cells Undergo Extensive Clonal Drift during Tissue Growth via Meox1-Mediated Induction of G2 Cell-Cycle Arrest. Cell Stem Cell *21*, 107-119 e106. 10.1016/j.stem.2017.06.003.

Pan, Y.A., Freundlich, T., Weissman, T.A., Schoppik, D., Wang, X.C., Zimmerman, S., Ciruna, B., Sanes, J.R., Lichtman, J.W., and Schier, A.F. (2013). Zebrabow: multispectral cell labeling for cell tracing and lineage analysis in zebrafish. Development *140*, 2835-2846. 10.1242/dev.094631.

Patton, E.E., Mueller, K.L., Adams, D.J., Anandasabapathy, N., Aplin, A.E., Bertolotto, C., Bosenberg, M., Ceol, C.J., Burd, C.E., Chi, P., et al. (2021). Melanoma models for the next generation of therapies. Cancer Cell *39*, 610-631. 10.1016/j.ccell.2021.01.011.

Patton, E.E., Widlund, H.R., Kutok, J.L., Kopani, K.R., Amatruda, J.F., Murphey, R.D., Berghmans, S., Mayhall, E.A., Traver, D., Fletcher, C.D., et al. (2005). BRAF mutations are sufficient to promote nevi formation and cooperate with p53 in the genesis of melanoma. Curr Biol *15*, 249-254. 10.1016/j.cub.2005.01.031.

Pinzon-Olejua, A., Welte, C., Chekuru, A., Bosak, V., Brand, M., Hans, S., and Stuermer, C.A. (2017). Cre-inducible site-specific recombination in zebrafish oligodendrocytes. Dev Dyn *246*, 41-49. 10.1002/dvdy.24458.

Pirici, D., Mogoanta, L., Kumar-Singh, S., Pirici, I., Margaritescu, C., Simionescu, C., and Stanescu, R. (2009). Antibody elution method for multiple immunohistochemistry on primary antibodies raised in the same species and of the same subtype. J Histochem Cytochem *57*, 567-575. 10.1369/jhc.2009.953240.

R-Core-Team (2020). R: A language and environment for statistical computing. R Foundation for Statistical Computing.

Rambow, F., Marine, J.C., and Goding, C.R. (2019). Melanoma plasticity and phenotypic diversity: therapeutic barriers and opportunities. Genes Dev *33*, 1295-1318. 10.1101/gad.329771.119.

Rambow, F., Rogiers, A., Marin-Bejar, O., Aibar, S., Femel, J., Dewaele, M., Karras, P., Brown, D., Chang, Y.H., Debiec-Rychter, M., et al. (2018). Toward Minimal Residual Disease-Directed Therapy in Melanoma. Cell *174*, 843-855 e819. 10.1016/j.cell.2018.06.025.

RStudio-Team (2016). RStudio: Integrated Development for R. RStudio, Inc.

Schindelin, J., Arganda-Carreras, I., Frise, E., Kaynig, V., Longair, M., Pietzsch, T., Preibisch, S., Rueden, C., Saalfeld, S., Schmid, B., et al. (2012). Fiji: an open-source platform for biological-image analysis. Nat Methods *9*, 676-682. 10.1038/nmeth.2019.

Shen, S., Faouzi, S., Souquere, S., Roy, S., Routier, E., Libenciuc, C., Andre, F., Pierron, G., Scoazec, J.Y., and Robert, C. (2020a). Melanoma Persister Cells Are Tolerant to BRAF/MEK Inhibitors via ACOX1-Mediated Fatty Acid Oxidation. Cell Rep *33*, 108421. 10.1016/j.celrep.2020.108421.

Shen, S., Vagner, S., and Robert, C. (2020b). Persistent Cancer Cells: The Deadly Survivors. Cell *183*, 860-874. 10.1016/j.cell.2020.10.027.

Singh, A.P., Dinwiddie, A., Mahalwar, P., Schach, U., Linker, C., Irion, U., and Nusslein-Volhard, C. (2016). Pigment Cell Progenitors in Zebrafish Remain Multipotent through Metamorphosis. Dev Cell *38*, 316-330. 10.1016/j.devcel.2016.06.020.

Than-Trong, E., Kiani, B., Dray, N., Ortica, S., Simons, B., Rulands, S., Alunni, A., and Bally-Cuif, L. (2020). Lineage hierarchies and stochasticity ensure the long-term maintenance of adult neural stem cells. Sci Adv *6*, eaaz5424. 10.1126/sciadv.aaz5424.

Thunemann, M., Schorg, B.F., Feil, S., Lin, Y., Voelkl, J., Golla, M., Vachaviolos, A., Kohlhofer, U., Quintanilla-Martinez, L., Olbrich, M., et al. (2017). Cre/lox-assisted non-invasive in vivo tracking of specific cell populations by positron emission tomography. Nat Commun *8*, 444. 10.1038/s41467-017-00482-y.

Tirosh, I., Izar, B., Prakadan, S.M., Wadsworth, M.H., 2nd, Treacy, D., Trombetta, J.J., Rotem, A., Rodman, C., Lian, C., Murphy, G., et al. (2016). Dissecting the multicellular ecosystem of metastatic melanoma by single-cell RNA-seq. Science *352*, 189-196. 10.1126/science.aad0501.

Tornini, V.A., Thompson, J.D., Allen, R.L., and Poss, K.D. (2017). Live fate-mapping of joint-associated fibroblasts visualizes expansion of cell contributions during zebrafish fin regeneration. Development *144*, 2889-2895. 10.1242/dev.155655.

Travnickova, J., and Patton, E.E. (2021). Deciphering Melanoma Cell States and Plasticity with Zebrafish Models. J Invest Dermatol *141*, 1389-1394. 10.1016/j.jid.2020.12.007.

Travnickova, J., Wojciechowska, S., Khamseh, A., Gautier, P., Brown, D.V., Lefevre, T., Brombin, A., Ewing, A., Capper, A., Spitzer, M., et al. (2019). Zebrafish MITF-Low Melanoma Subtype Models Reveal Transcriptional Subclusters and MITF-Independent Residual Disease. Cancer Res *79*, 5769-5784. 10.1158/0008-5472.CAN-19-0037.

Tsujikawa, T., Kumar, S., Borkar, R.N., Azimi, V., Thibault, G., Chang, Y.H., Balter, A., Kawashima, R., Choe, G., Sauer, D., et al. (2017). Quantitative Multiplex Immunohistochemistry Reveals Myeloid-Inflamed Tumor-Immune Complexity Associated with Poor Prognosis. Cell Rep *19*, 203-217. 10.1016/j.celrep.2017.03.037.

Vendramin, R., Katopodi, V., Cinque, S., Konnova, A., Knezevic, Z., Adnane, S., Verheyden, Y., Karras, P., Demesmaeker, E., Bosisio, F.M., et al. (2021). Activation of the integrated stress response confers vulnerability to mitoribosome-targeting antibiotics in melanoma. J Exp Med *218*. 10.1084/jem.20210571.

Wang, L., Wang, S., Yin, J.J., Fu, P.P., and Yu, H. (2009). Light-Induced Toxic Effects of Tamoxifen: A Chemotherapeutic and Chemopreventive Agent. J Photochem Photobiol A Chem *201*, 50-56. 10.1016/j.jphotochem.2008.09.013.

Wickham, H. (2016). ggplot2: Elegant Graphics for Data Analysis. Spinger-Verlag.

Wojciechowska, S., van Rooijen, E., Ceol, C., Patton, E.E., and White, R.M. (2016). Generation and analysis of zebrafish melanoma models. Methods Cell Biol *134*, 531-549. 10.1016/bs.mcb.2016.03.008.

Wouters, J., Kalender-Atak, Z., Minnoye, L., Spanier, K.I., De Waegeneer, M., Bravo Gonzalez-Blas, C., Mauduit, D., Davie, K., Hulselmans, G., Najem, A., et al. (2020). Robust gene expression programs underlie recurrent cell states and phenotype switching in melanoma. Nat Cell Biol *22*, 986-998. 10.1038/s41556-020-0547-3.

Zeng, Z., Johnson, S.L., Lister, J.A., and Patton, E.E. (2015). Temperature-sensitive splicing of mitfa by an intron mutation in zebrafish. Pigment Cell Melanoma Res *28*, 229-232. 10.1111/pcmr.12336.

Figure Legends

Figure 1: Tamoxifen inducible *cre^{ERt2}/loxP* system in zebrafish.

A. A schematic of *mitfa:cre^{ERt2}* and *ubi:Switch* (Mosimann et al., 2011) constructs to enable green-to-red switch in *mitfa* promoter expressing cells after tamoxifen treatment. The cardiac myosin light chain (cmlc) 2 promoter drives GFP expression and facilitates screening for the cre^{ERt2} line based on GFP+ heart myocardium. mCh: mCherry.

B. A schematic of the concept behind the colour switching *cre^{ERt2}/loxP* system that allows green-to-red switch after tamoxifen treatment in cells expressing the promoter driving *cre*. Left: A three-night-course treatment with tamoxifen for 11-12 hours by immersion in dark with drug-free period during the day. Right: The principle of colour switch upon tamoxifen treatment as a result of Cre^{ERt2} trans-localisation to nucleus, causing excision of GFP and stop codon, enabling mCherry expression in recombined cells.

Figure 2: Successful fluorophore switch in the adult zebrafish primary melanoma after tamoxifen treatment

A. An illustration of the expected fluorophore switch in the primary melanoma tumour upon tamoxifen treatment.

B. An adult zebrafish with fully developed primary melanoma tumour (delineated with white dashed line) 2 days before the tamoxifen treatment course (left) and 6 days after the start of the treatment (right) showing *de novo* expression of mCherry protein in pigmented trunk tumour after tamoxifen treatment (4 μM, in magenta). N = 2 fish, Scale bar = 1 mm.

C.-D. Standard deviation intensity (STD) projections of confocal z-stacks of DMSO (0.04 %) treated fish (**C**, left mCherry, right merged with GFP) and tamoxifen treated fish (**D**, left mCherry, right merge) show small clusters of mCherry expressing cells in the tamoxifen treated group only (in magenta, white arrows). N = 2 fish, scale bar = 100 μm.

E.-F. Paraformaldehyde fixed paraffin embedded transverse sections of primary melanoma fish stained with haematoxylin and eosin with zoomed image of the tumour (red arrows pointing to the location of the right displays). N = 2 fish, scale bars = 2.5 mm and 100 μm respectively. Dashed boxes indicate area of section shown in **E'-F'** and **E''-F''**. **E'.-F'.** Immunofluorescence staining of bulk tumour with a mCherry antibody (magenta), counterstained with the nuclear marker DAPI (cyan), shows mCherry signal in tamoxifen treated samples only (**F'**) compared to DMSO control (**E'**). N = 2 fish, scale bar = 25 μm. **E''.-F''.** Immunofluorescence staining of invasive tumour show successful fluorophore switching and mCherry expression in the tamoxifen treated group (**F''**) compared to DMSO control (**E''**). N = 2 fish, scale bar = 25 μm.

G. A schematic of *mitfa:cre*^{ERt2} and *ubi:zebrabow* constructs which enable recombination from red signal (RFP) to a stochastic combination of cerulean (CFP), yellow (YFP) and red (RFP) signal in *mitfa:cre*^{ERt2} expressing cells after tamoxifen treatment. The cardiac myosin light

chain (cmlc) 2 promoter drives GFP expression and facilitates screening for the cre^{ERt2} line based on GFP+ heart myocardium.

H. An adult zebrafish with an early stage melanoma lesion 19 days after tamoxifen treatment (delineated with white dashed line) showing “switched” cells in cerulean (CFP) and yellow (YFP), bottom panels show RFP signal (in magenta) and merge of three channels (right bottom panel). Right panels then show an increase of YFP signal (in yellow, right middle panel) 87 days post treatment as the tumour progresses, N = 2 fish, Scale bar = 1 mm.

Figure 3: Persister cells originate from the primary tumour

A. The experimental workflow of tamoxifen treatment and melanoma regression at the higher water temperature (32°C, MITF OFF). At the higher temperature *mitfa* RNA is still expressed but is not spliced correctly and therefore MITF activity is abolished. Loss of MITF activity leads to tumour regression with remaining persister cells at the minimal residual disease (MRD) site.

B. A fish treated with vehicle (DMSO 0.05%) showing no green-to-red recombination in the primary tumour (top) or after regression (bottom). Scale bar = 1 mm, white arrow points at the tumour site, N = 4 fish.

C. A fish treated with tamoxifen (5 μM) showing expression of mCherry positive (magenta) cells in a primary tumour (top, white arrows) that are still detected after 59 days of melanoma regression (bottom, white arrows). Scale bar = 1 mm, N = 7 fish.

D. STD projections of confocal z-stack acquisitions of regression sites of fish treated with vehicle (DMSO, top row) or Tamoxifen (bottom row). White arrows point at mCherry positive cells (in magenta) only present in the tamoxifen treated condition. Scale bar = 50 um, DMSO: N = 4 fish; Tamoxifen: N = 7 fish.

E. Box plot of fluorescence intensity quantification of mCherry signal using average intensity projections of confocal images of residual disease comparing DMSO to Tamoxifen condition. DMSO: N = 4 fish with 7 regression sites; Tamoxifen: N = 7 fish with 9 regression sites; ** $p<0.01$, Wilcoxon test.

F. Immunohistochemistry of regressed zebrafish FFPE transverse section to target mCherry protein of "switched" cells, right panel shows an enlarged view of black dashed rectangle (left panel) capturing the residual disease site. Signal in red (AEC substrate) counterstained with nuclear marker haematoxylin. Scale bar= 50 μm, N = 3 fish.

Figure 4: Successful GFP to mCherry fluorophore switch in persister cells

A. Schematic representation of experimental workflow of tamoxifen treatment of regressed fish. Red arrow highlights location of recombined melanoma cells at minimal residual disease site.

B. A regressed fish treated with vehicle (DMSO 0.04% at 31-32°C) showing no green-to-red recombination in the melanoma minimal residual disease (bottom) compared to pre-treatment image (middle). Scale bar = 1 mm, N = 3 fish.

C. A regressed fish treated with Tamoxifen (4 μM, at 32°C) showing mCherry positive cells (in magenta) in the melanoma minimal residual disease compared to pre-treatment image (middle). Scale bar = 1 mm, N = 3 fish.

D. STD projections of confocal z-stack acquisitions showing regression sites of fish treated with vehicle (DMSO, top row) or Tamoxifen (bottom row) of regressed treated fish. White arrows point at little clusters of mCherry positive cells (in magenta) present only in tamoxifen treated condition. Scale bar = 50 um, N = 3 fish.

Figure 5: Persister cells directly contribute to melanoma recurrent disease

A. A fish with a regressed melanoma (top image: primary tumour; below: regressed tumour) treated with vehicle (DMSO 0.04-0.05% at 32 °C) showing no green-to-red fluorophore switch in the melanoma minimal residual disease compared to pre-treatment image. Follow–up bright field and fluorescent acquisitions (every 14 days) show progression of tumour recurrence over time with no appearance or increase of mCherry fluorescence (in magenta). Scale bar = 1mm. N= 5 fish (sum of two independent experiments).

B. A fish with a regressed melanoma (top image: primary tumour; below: regressed tumour) treated with 4-5 μM tamoxifen (at 32 °C) showing green-to-red fluorophore switch (in magenta) in the melanoma minimal residual disease compared to pre-treatment image. Follow–up brightfield and fluorescent acquisitions (every 14 days) show progression of tumour recurrence over time with increasing mCherry signal. Scale bar = 1 mm. N = 7 fish (sum of two independent experiments).

C. STD projections of z-stack confocal acquisition show recurred melanoma sites of fish treated with vehicle (DMSO, top row) or Tamoxifen (bottom row) during minimal residual disease time point and recurred prior confocal imaging. Scale bar = 100 um.

D. Box plot of fluorescence intensity quantification of mCherry signal using average intensity projections of confocal images of residual disease comparing DMSO to Tamoxifen condition. DMSO: N=3 fish; Tamoxifen treated group: N=4 fish with 7 recurred melanomas * $p<0.05$, Wilcoxon test.

E. A representative pseudocolour flow cytometry plot of a recurred melanoma lesion from DMSO treated fish (left) and tamoxifen treated fish (right). mCherry positive cells highlighted in red rectangle (12.3% vs 0.062%). DMSO: N= 4 fish; Tamoxifen: N = 5 fish (sum of two independent experiments).

Figure 6: MITF-independent persister cells regain Mitfa protein expression in recurrent disease.

A. Overview of the multiplex immunohistochemistry protocol. The antibody staining is repeatedly imaged and stripped, images are pseudocoloured and stacked on ImageJ to generate composite image.

B. Overview of DMSO treated melanoma recurrent disease on top of head, showing Sox10, mCherry and Mitf protein staining overlaid with haematoxylin counterstain, dashed white box indicates area of section shown in **B'**. Scale bar, 250 µm.

B'. Enlarged views of DMSO treated tumour section shown in **B**, showing lack of mCherry staining in melanoma cells positive for Sox10 and Mitf. Scale bar, 50 µm. Unspecific mCherry signal does not represent staining of tumour cells, rather trapped antibody in detached tissue fragments.

C. (Left, top to bottom) brightfield images of melanoma tail fin tumour through growth, regression and recurrence. (Right, middle and bottom) fluorescent images of regressed and recurred melanoma tail fin tumour, showing mCherry fluorescence in the recurred tumour following tamoxifen mediated recombination. Scale bars, 500 µm.

D. Overview of tamoxifen treated melanoma recurrent disease in the tail fin, showing Sox10, mCherry and Mitf protein staining overlaid with haematoxylin counterstain, dashed white box indicates area of section shown in **D'**. Scale bar, 250 µm.

D'. Enlarged views of tumour section shown in **D**, showing individual staining of Sox10, Mitf, and mCherry proteins. Scale bar, 50 µm. White arrows highlight cells positive for Sox10, Mitf and mCherry staining.

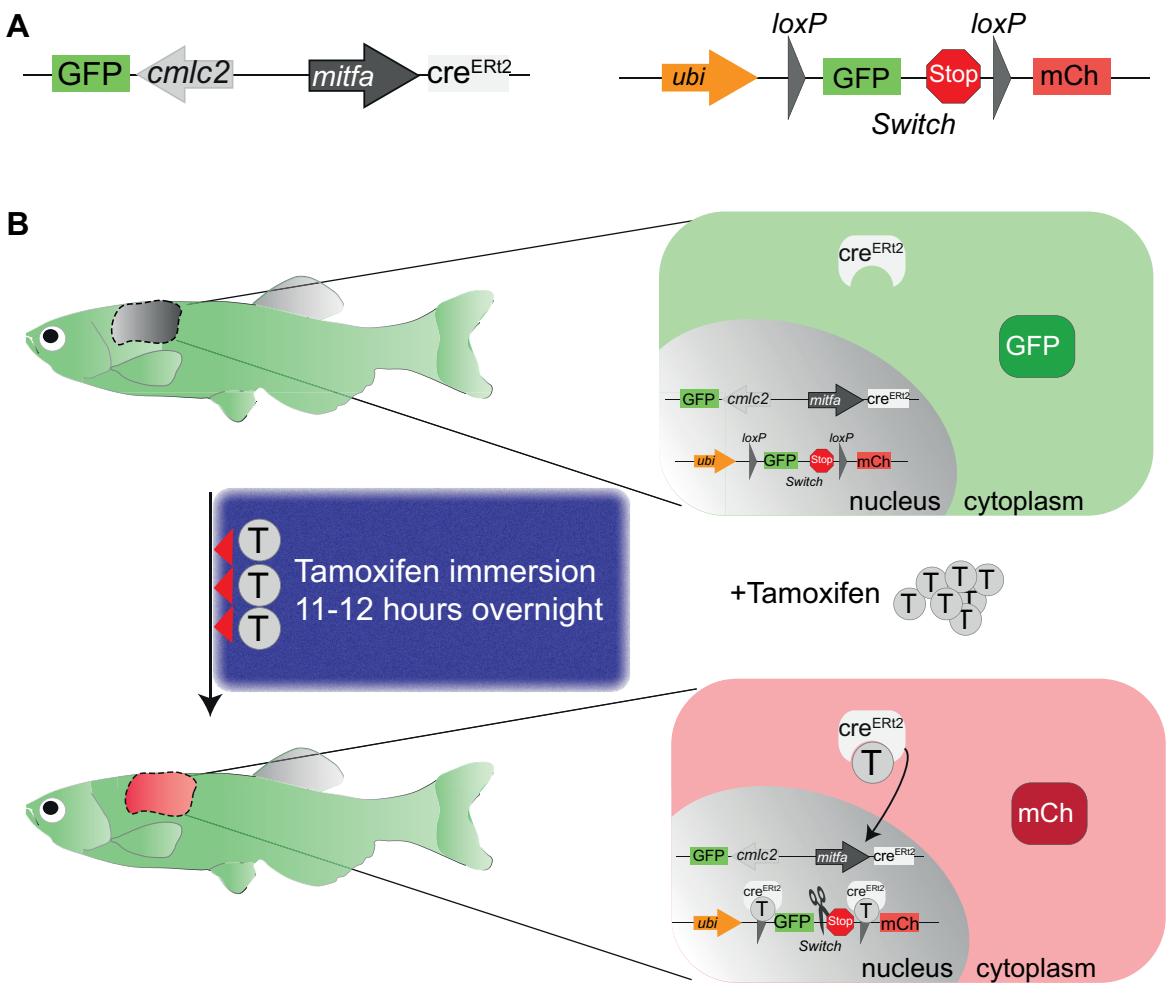

Travnickova *et al*, Figure 1

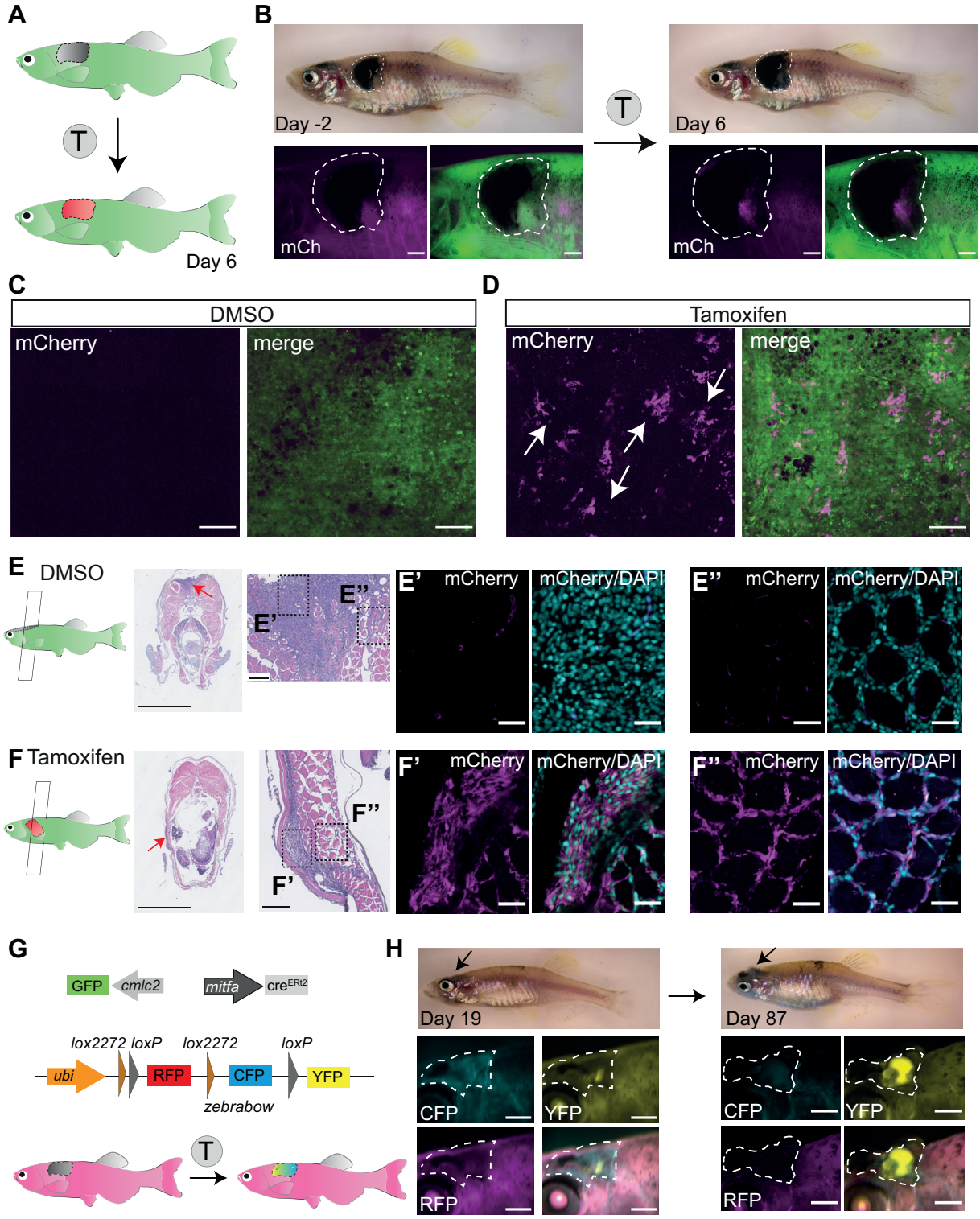

Travnickova *et al*, Figure 2

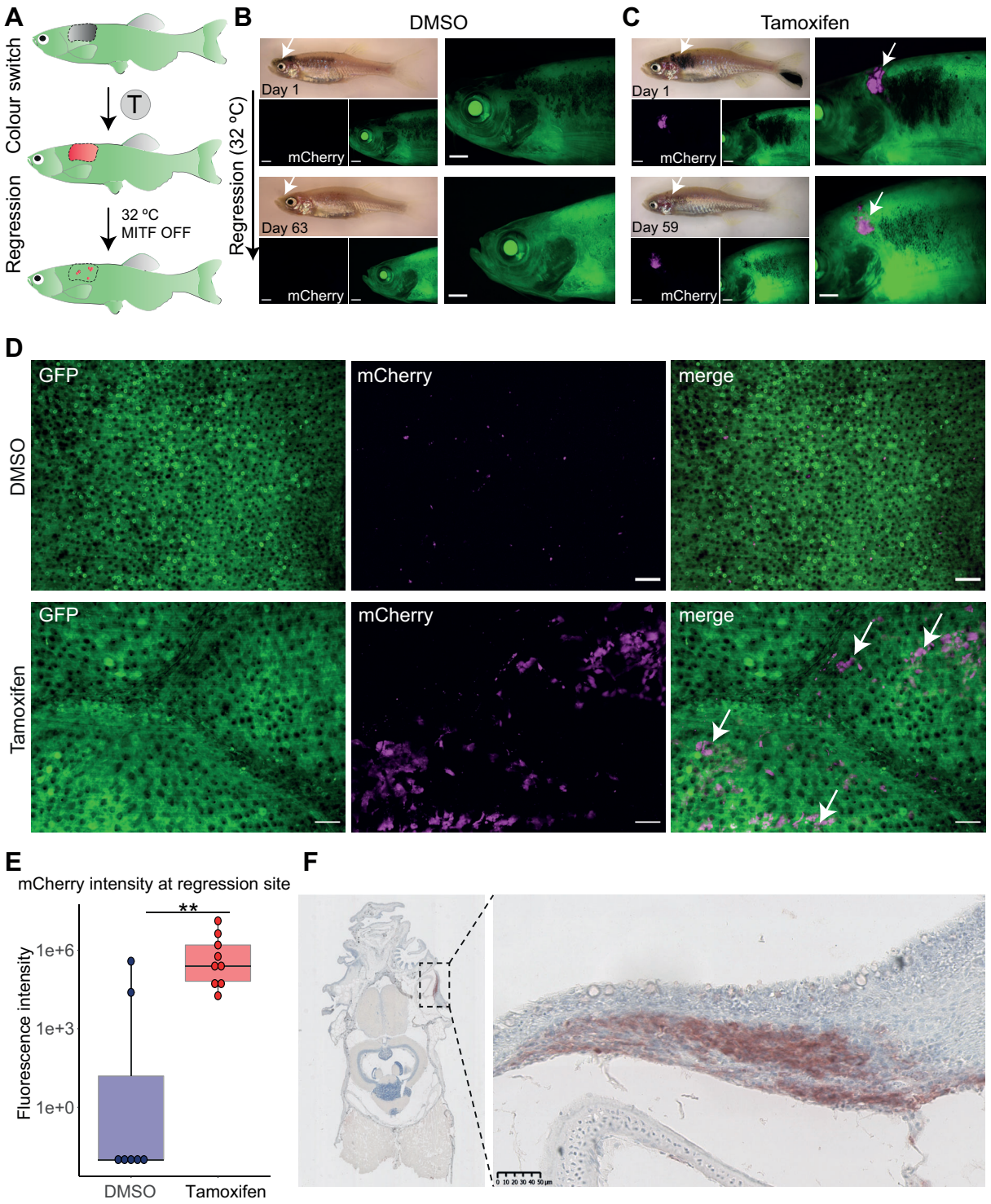

Travnickova *et al*, Figure 3

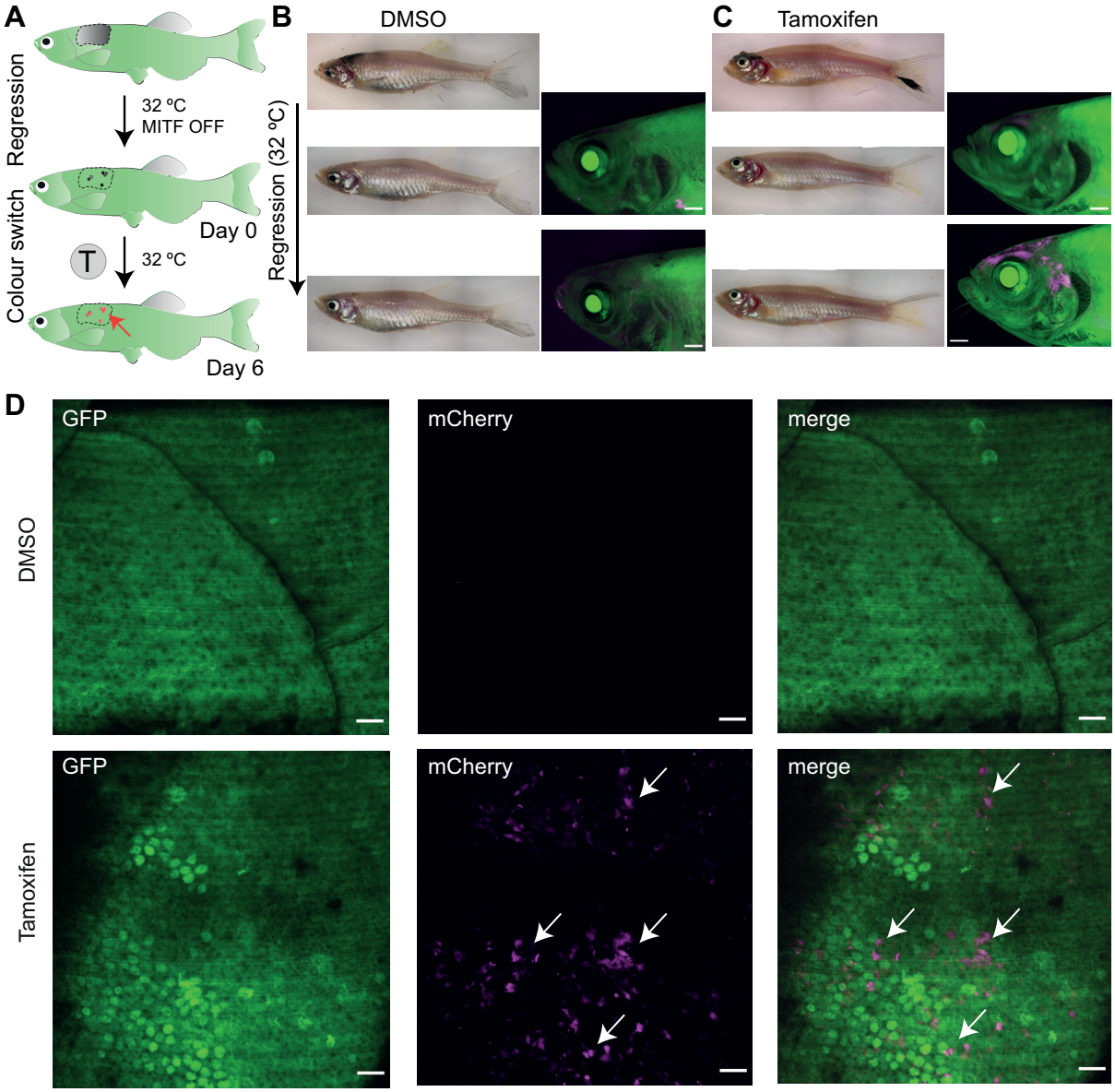

Travnickova *et al*, Figure 4

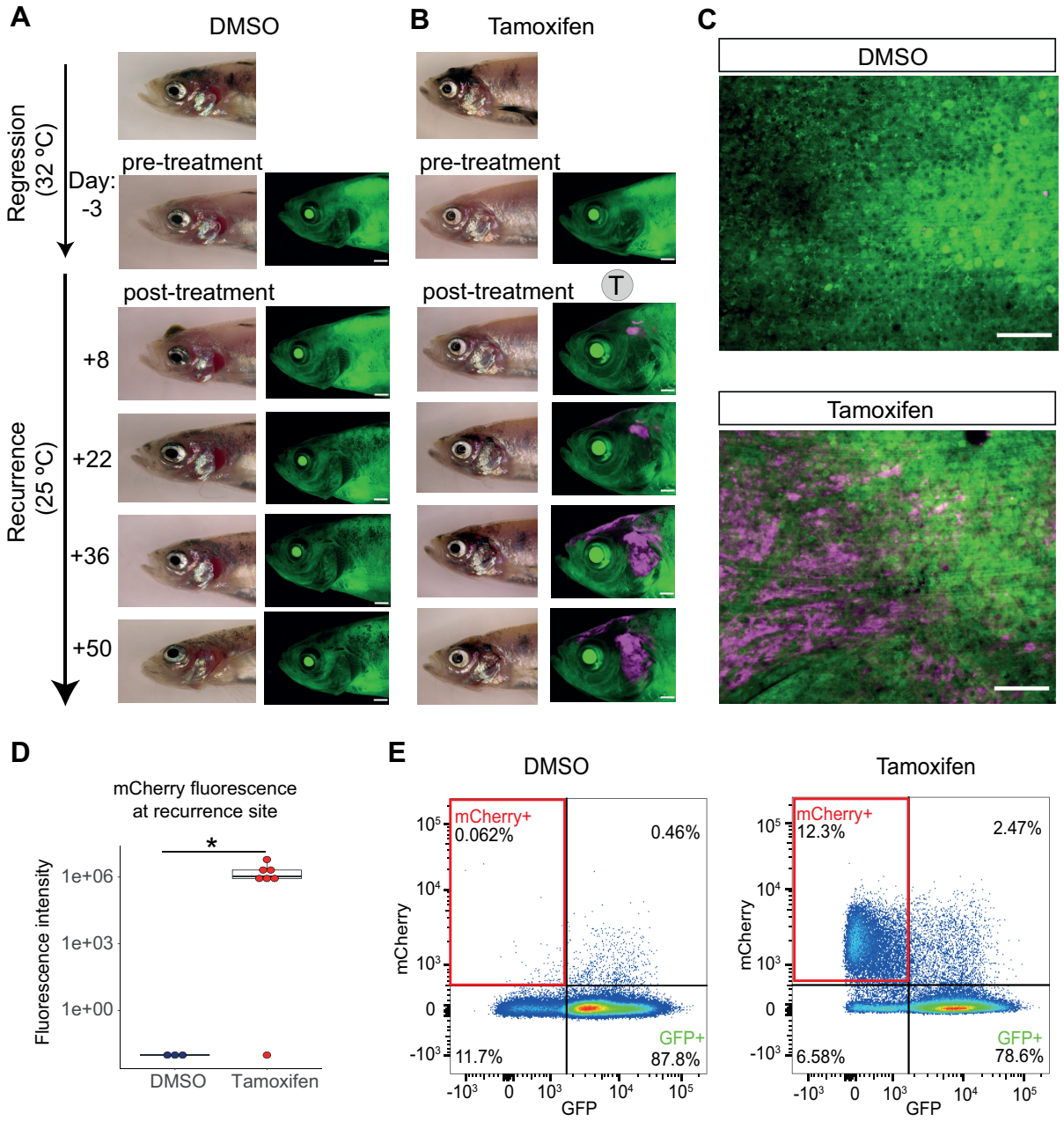

Travnickova *et al*, Figure 5

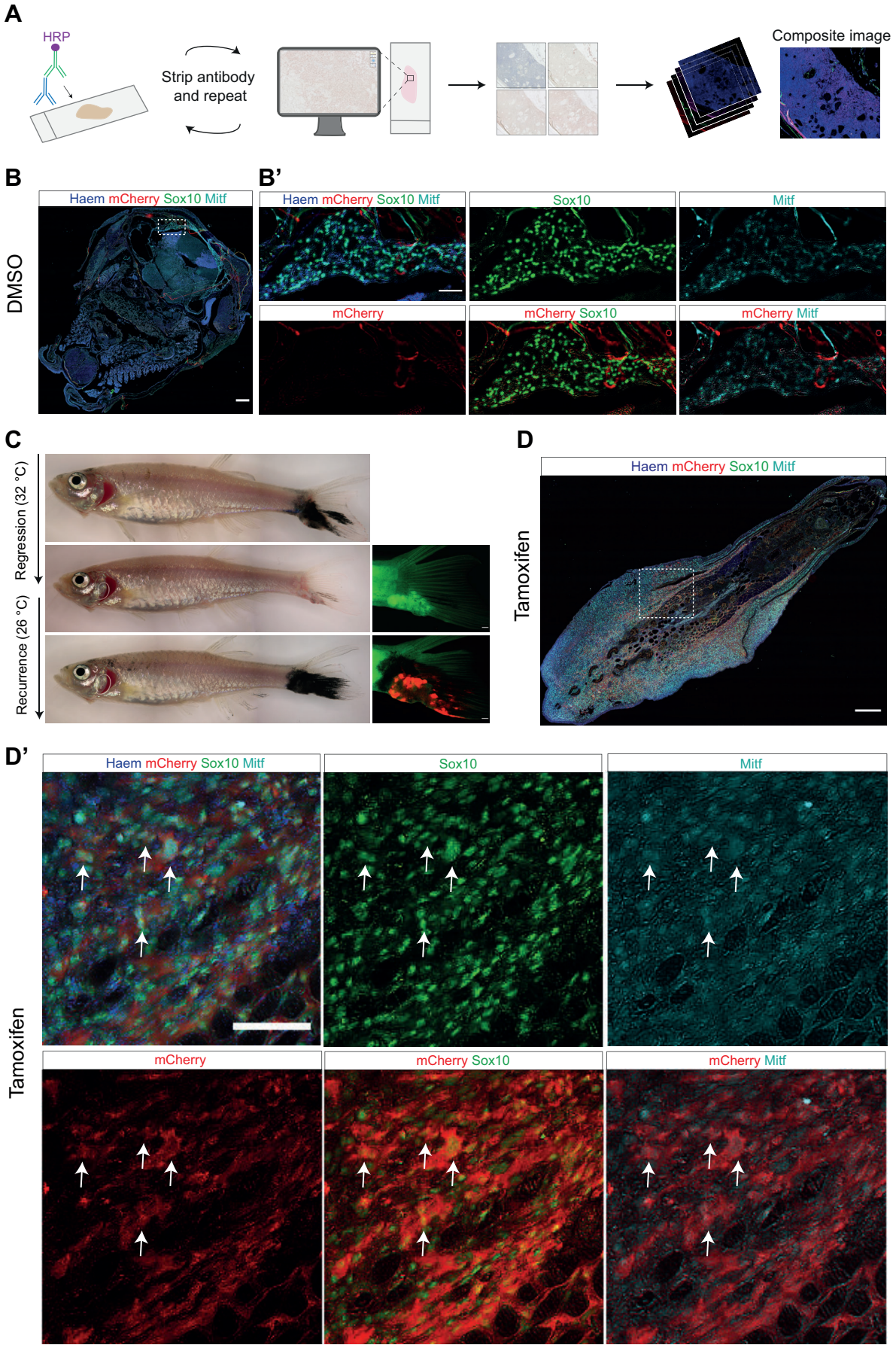

Travnickova *et al*, Figure 6